

THE VELOCITY FIELD PREDICTED BY THE OPTICAL REDSHIFT SURVEY

JONATHAN E. BAKER AND MARC DAVIS

Astronomy Department, University of California, Berkeley, CA 94720;
 jrbaker@astro.berkeley.edu

MICHAEL A. STRAUSS¹

Princeton University Observatory, Princeton, NJ 08544

OFER LAHAV

Institute of Astronomy, Cambridge University, Madingley Road, Cambridge CB3 0HA,
 United Kingdom

AND

BASÍLIO X. SANTIAGO

Departamento de Astronomia, Universidade Federal do Rio Grande do Sul, 91501-970, Porto Alegre, RS,
 Brasil

Draft version December 2, 2024

ABSTRACT

We have used the Optical Redshift Survey (ORS; Santiago et al. 1995) to construct the gravity field due to fluctuations in the galaxy density field out to distances of 8000 km s⁻¹. At large scales where linear theory applies, the comparison of this gravity field with the observed peculiar velocity field offers a powerful cosmological probe, because the predicted flow field is proportional to the parameter $\Omega^{0.6}/b$, where Ω is the matter density and b is the bias of the galaxy distribution. The more densely sampled ORS gravity field, to excellent approximation, matches that of the earlier *IRAS* 1.2-Jy redshift survey (Fisher et al. 1995a), provided β is reduced by a factor $b_{opt}/b_{IRAS} \approx 1.4$. Apart from this scaling, the most significant difference between the ORS and *IRAS* fields is induced by differing estimates of the over-density of the Virgo cluster. Neither of these gravity fields is consistent with the peculiar velocity field constructed from the full Mark III (Willick et al. 1997a) sample. We find that a simple but plausible non-linear bias algorithm for the galaxy distribution relative to the mass has a negligible effect on the derived fields. We conclude that the substitution of optical for *IRAS* catalogues cannot alone resolve the discrepancies between the *IRAS* gravity field and the Mark III peculiar velocity field.

Subject headings: cosmology — dark matter — galaxies: clustering — large-scale structure of universe

1. INTRODUCTION

With the advent of large, uniform redshift surveys of galaxies, increasingly stringent tests of models for the large-scale structure of the universe have become possible (see, e.g., Dekel 1994 and Strauss & Willick 1995 for reviews). Under the assumption that large-scale flows of galaxies in the universe are a response to the underlying distribution of matter, peculiar velocity measurements are a critical probe of cosmology and large-scale structure. Redshift surveys allow one to construct an estimate of the gravity field based on the observed distribution of galaxies. Using linear or quasi-linear gravitational instability theory, one can predict the velocity field from this gravity field, a prediction which is approximately proportional to the parameter $\beta \equiv f(\Omega)/b$, where b is the galaxy bias, f is a function which is well approximated by $\Omega^{0.6}$ (Peebles 1980), and Ω is the matter density.

Until recently, the Infrared Astronomical Satellite (*IRAS*) 1.2-Jy flux-limited redshift survey was the only available nearly full-sky catalogue. The original redshift survey of *IRAS*-selected galaxies was limited to a sample of 2658 galaxies with 60-micron flux greater 1.936 Jy (Strauss et al. 1992a), but this was later extended to a sample of 5321 galaxies brighter than 1.2 Jy (Fisher et al. 1995a). A sample of 13,000 galaxies complete to 0.6 Jy is

nearing completion (Canavezes et al. 1998) and is eagerly awaited. The principal advantage of these *IRAS*-selected samples is their insensitivity to extinction within the Milky Way, allowing extremely large sky coverage, 87.6% (11.01 sr) for the 1.2-Jy sample, with a single, linear instrument. Nearly full-sky coverage is essential for estimation of the peculiar gravity field.

However, it is well known that the distribution of *IRAS* galaxies is biased with respect to the overall distribution of galaxies (Strauss et al. 1992b), primarily because *IRAS* under-counts the dust-free early-type galaxies which congregate in cluster centers. The *IRAS* surveys are also more dilute than is desirable, typically including only 1/3 of the known spiral galaxies in volumes where the selection function is high. Optically-selected surveys can eliminate this bias, and deeper redshift surveys will overcome the shot noise problem associated with the sparse sampling of the *IRAS* survey. The recently completed Optical Redshift Survey (ORS; Santiago et al. 1995) is currently the best available catalogue for our peculiar velocity analysis. The ORS is a concatenation of three optically-selected samples covering most of the sky with $|b| > 20^\circ$, and it is the best current approximation to a full-sky optically-selected catalogue. Until a redshift catalogue is constructed from the 2MASS survey (Stiening, Skrutski, & Capps 1995), the

¹Alfred P. Sloan Foundation Fellow, and Cottrell Scholar of Research Corporation

ORS is likely to remain the closest competitor to the *IRAS* full-sky catalogue. Previous work (Freudling, da Costa, & Pellegrini 1994) suggests that the *IRAS* and optical gravity fields are consistent, but with the superior data now available, it is clearly of interest to determine the nature of any deviations between the gravity fields of the optical and *IRAS* samples, as these could substantially affect comparisons to observed peculiar velocity fields. Direct density field comparisons (Santiago & Strauss 1992; Strauss et al. 1992b) between the ORS and other redshift surveys will be carried out in detail by Strauss et al. (1998).

Comparisons of the gravity field derived from the *IRAS* survey with observed peculiar velocity samples have been carried out using a number of complementary methods (see Strauss & Willick 1995 for a review), with more recent studies performed by Davis, Nusser, & Willick (1996; hereafter, DNW96), Willick et al. (1997b), Riess et al. (1997), Sigad et al. (1998), da Costa et al. (1998), and Willick & Strauss (1998). These studies show that the *IRAS*-predicted flow field is at least qualitatively very similar to the measured velocity field, lending strong support to the gravitational instability model for the growth of large-scale structure. Although the qualitative alignment of the *IRAS*-predicted and Mark III peculiar velocity fields is remarkably good, detailed quantitative comparisons are, at present, less satisfactory. DNW96 find large coherent residuals between the *IRAS* and Mark III fields, primarily in the dipole component at large scales, which preclude a conclusive determination of β . Willick et al. (1997b) find better alignment of the *IRAS* gravity and Mark III velocity fields using the rather different VELMOD technique, but this analysis is limited to redshifts within 3000 km s^{-1} ; Willick & Strauss (1998) find good agreement on larger scales, but conclude that this requires a re-calibration of the Tully-Fisher relations for the various subsamples going into the Mark III catalogue inconsistent with the published calibration (Willick et al. 1997a). On the other hand, da Costa et al. (1998) find a better match between the large-scale *IRAS* gravity field and the SFI I-band sample of spiral field galaxy peculiar velocity measurements (Giovannelli et al. 1997). The SFI sample uses the same Mathewson, Ford, & Buchhorn (1992) data for the Southern sky as in Mark III, but the transformation of the data to a common system differs from the Mark III treatment. A recent summary of the current confusion is given by Davis (1998). Might some of the discrepancy disappear if we were to use an optical redshift survey to construct an estimate of the gravity field?

This paper addresses the question of the construction of a three-dimensional gravity field based on the ORS and *IRAS* redshift catalogues. We construct our estimate of the gravity field using the redshift-space procedure described by Nusser & Davis (1994). Section 2 describes the galaxy catalogues and our procedure for merging them. The method for obtaining the gravity and velocity fields is briefly outlined in §3, with details of the spherical harmonic formalism in the Appendix; more details have been presented elsewhere. Section 4 describes the differences between the ORS field and the field derived from *IRAS* alone, including a brief discussion of alternatives to the simple linear biasing scheme, and §5 discusses the main conclusions.

2. THE GALAXY CATALOGUES

The Optical Redshift Survey (ORS) is a combination of three individual declination-limited catalogues: the Uppsala General Catalogue (UGC) at northern declinations ($\delta \geq -2.5^\circ$), the European Southern Observatory (ESO) catalogue in the south ($\delta < -17.5^\circ$), and the Extension to the Southern Observatory Catalogue (ESGC) in the remaining strip just south of the Celestial Equator. The sample selection and galaxy distribution have been described in detail (Santiago et al. 1995), and the selection functions for the galaxies in each sample have been carefully calibrated (Santiago et al. 1996). We use the flux-limited versions of the UGC and ESO catalogues; for the ESGC catalogue, only a diameter-limited sample was available. All velocities have been converted to the Local Group (LG) frame using the transformation of Yahil, Tammann & Sandage (1977).

Hudson (1993a, 1993b) constructed a full-sky map of the local density field from optically-selected galaxies, using the UGC and ESO catalogues limited to a redshift of 8000 km s^{-1} . Complete redshift information did not exist for these catalogues at the time of his analysis, and his sky coverage was limited to 67%. Furthermore, his procedure for merging the UGC and ESO into a single catalogue may have led to spurious asymmetries between the North and South. The complete ORS redshift sample allows us to overcome many of these limitations.

Our analysis relies on a spherical harmonic expansion of the density field and therefore requires data of uniform quality over the entire sky. Unfortunately, there are several limitations which prevent the ORS from being a uniform, all-sky survey. Because the ORS galaxies are optically selected, the catalogue is affected much more adversely by extinction than is the *IRAS* survey. The ORS does not cover the strip at Galactic latitudes $|b| < 20^\circ$, while the *IRAS* survey excludes only the strip with $|b| < 5^\circ$, two small unobserved strips at higher latitudes, and small confusion-limited regions (about 12.4% of the sky in total). In addition, we only use ORS data in regions where the Burstein & Heiles (1984) blue extinction is low: $A_B < 0.7$ magnitudes. Finally, there are 64 plates, each 5° on a side, which are missing from the ESO-LV survey (Fig. 5a of Santiago et al. 1995). The accepted ORS data cover about 62% of the sky, and the completeness of the catalogues within these regions is excellent.

To produce an all-sky catalogue, we use the *IRAS* survey to fill in the areas in which ORS data are absent or the extinction is high. The *IRAS* catalogue (Fisher et al. 1995a) contains 5321 galaxies covering 87.6% of the sky. We use a version of this catalogue which Yahil et al. (1991) have carefully augmented with fake galaxies in the Zone of Avoidance (and other excluded regions) without biasing the statistics of the galaxy distribution. This all-sky *IRAS* catalogue contains 6010 galaxies. The *IRAS* data are only used in regions where there are no accepted ORS data, so each of the four surveys cover disjoint regions on the sky.

The ORS survey has the advantage that it is much more densely sampled than the *IRAS* survey within $cz \sim 8000 \text{ km s}^{-1}$. This allows the local gravity and velocity fields to be constructed with much smaller sampling errors. However, the ORS selection function drops exponentially with distance, while the *IRAS* galaxy distribution

has a long power-law tail extending to higher redshifts. Beyond 8000 km s⁻¹, the ORS data become unacceptably sparse. We therefore use only *IRAS* data over the whole sky for redshifts $cz > 8000$ km s⁻¹, extending the analysis to $cz = 18,000$ km s⁻¹.

To generate a density field in redshift space, we first merge the galaxy catalogues into a single, all-sky, uniform catalogue. Each catalogue j has a selection function ϕ_j such that for homogeneously distributed galaxies, the expected galaxy density at a point $\mathbf{s} = (s, \theta, \varphi)$ is $\bar{n}_j \phi_j(\mathbf{s})$, where \bar{n}_j is the true average density of galaxies in the catalogue volume. Since we are given the selection functions ϕ_j (Santiago et al. 1996), we calculate the density in (some part of) the volume of catalogue j using

$$\bar{n}_j = \frac{1}{V_j} \sum_{i \in j} \frac{1}{\phi_j(\mathbf{s}_i)}, \quad (1)$$

where the sum is over galaxies i in the volume of interest. The sky coverage Ω_j of each of the surveys is known (Santiago et al. 1995), so

$$V_j = \frac{1}{3} \Omega_j s_{max,j}^3 \quad (2)$$

is known. Galaxies with $s_i > s_{max,j}$ are not included in the analysis. We calculate the density within $s_{max} = 8000$ km s⁻¹ for the three ORS catalogues and the *IRAS* catalogue, although, as mentioned above, the *IRAS* analysis is carried out to 18,000 km s⁻¹. The densities we compute are for objects sufficiently luminous to be included in a volume-limited sample out to radius $cz = 500$ km s⁻¹.

The fractional density fluctuation is given by the ratio of the observed galaxy counts to the number expected given the selection function. This can be calculated by assigning each galaxy i a weight $[\bar{n}_j \phi_j(\mathbf{s}_i)]^{-1}$. In our merged catalogue, we multiply these weights by factors which normalize the density in each catalogue to the density of *IRAS* galaxies *within the accepted volume of the optical subsample*. This allows each ORS subsample to have a density which, due to inhomogeneities, is not necessarily the same as the overall density, but it matches the different ORS subsamples to the uniformly-selected *IRAS* catalogue. Thus we calculate $\bar{n}_{IRAS,j}$, the density of *IRAS* galaxies within the volume of catalogue j , relative to \bar{n}_{IRAS} , the overall density of *IRAS* galaxies. The weight for any galaxy is then given by

$$W_i = \frac{1}{\bar{n}_j \phi_j(\mathbf{s}_i)} \frac{\bar{n}_{IRAS,j}}{\bar{n}_{IRAS}}. \quad (3)$$

This weighting ensures that the density of the merged catalogue remains approximately constant across catalogue boundaries. Some parameters of the catalogues are listed in Table 1 (cf. Santiago et al. 1996).

3. CALCULATION OF THE VELOCITY FIELD

Nusser & Davis (1994) show that in linear theory, the peculiar velocity field in redshift space is irrotational and can therefore be derived from a potential: $\mathbf{v}(\mathbf{s}) = -\nabla\Phi(\mathbf{s})$. If the angular dependences of the potential and galaxy density field $\delta^g \equiv \delta\rho^g/\bar{\rho}^g$ (both measured in redshift space)

are expanded in terms of spherical harmonics as described in Appendix A, the potential is related to the density field by

$$\frac{1}{s^2} \frac{d}{ds} \left(s^2 \frac{d\Phi_{lm}}{ds} \right) - \frac{1}{1+\beta} \frac{l(l+1)\Phi_{lm}}{s^2} = \frac{\beta}{1+\beta} \left(\delta_{lm}^g - \frac{1}{s} \frac{d \ln \phi}{d \ln s} \frac{d\Phi_{lm}}{ds} \right). \quad (4)$$

This is a modified Poisson equation, where δ_{lm}^g is the spherical harmonic coefficient of the redshift-space galaxy density field, s is the redshift, and β was defined above. The last term on the right hand side corrects for the “rocket effect”, which arises because we weight each galaxy by the selection function ϕ evaluated at its redshift rather than its (unknown) distance.

We now briefly summarize our computationally efficient method for solving the above equation. We first compute a smoothed density field on a spherical grid in redshift space. We construct a 32×32 angular grid equally spaced in Galactic longitude and latitude, with 52 bins in redshift out to 18,000 km s⁻¹, providing more than adequate resolution given the smoothing of the fields. The separation of the redshift bins increases in proportion to the mean *IRAS* inter-particle spacing, $(\bar{n}\phi)^{-1/3}$, in order to reflect the decreased sensitivity of the surveys at high redshift. The Gaussian-smoothed galaxy density field at grid point n is given by

$$1 + \delta^g(\mathbf{s}_n) = \frac{1}{(2\pi)^{3/2} \sigma_n^3} \sum_i W_i e^{-(\mathbf{s}_n - \mathbf{s}_i)^2 / 2\sigma_n^2}, \quad (5)$$

where the sum is over all galaxies in the merged catalogue. The Gaussian smoothing width for the cell, σ_n , is equal to the mean *IRAS* inter-particle spacing at that redshift (or 100 km s⁻¹ when the inter-particle spacing is smaller than this). The increased smoothing at larger redshifts is essential to prevent divergence of the increasing shot noise; our procedure is qualitatively close to the optimal Wiener filtering procedure (Lahav et al. 1994; Fisher et al. 1995b), and the result is a signal-to-noise ratio in the density field that is roughly constant over radial bins. A correction factor must also be applied because part of the Gaussian-weighted volume centered on a cell will fall outside the survey cutoff radius.

The spherical harmonic coefficients of the density field are calculated on radial (redshift) shells. Once these coefficients δ_{lm}^g have been computed for the merged catalogue, the modified Poisson equation for the potential is solved. The velocity field can then easily be constructed from $\mathbf{v} = -\nabla\Phi$.

Our analysis is done purely in redshift space, assuming linear theory and a one-to-one mapping between distance and redshift along any given line of sight. These assumptions become invalid in clusters, where highly nonlinear, virialized motions cause a radial distortions into “fingers of God.” We follow Yahil et al. (1991) in collapsing the galaxies in the six nearest clusters of their Table 2 to a single redshift.

A limitation of the density field constructed by merging disparate catalogues is that we can only use one selection function for the $d \ln \phi / ds$ term on the right hand side of the modified Poisson equation (see Appendix B

Catalogue	Sky coverage	N_{gal} (total)	N_{gal} (used)	\bar{n}_j ($h^3 \text{ Mpc}^{-3}$)	$\bar{n}_{IRAS,j}$	$\bar{n}_{IRAS,j}/\bar{n}_{IRAS}$
<i>IRAS</i>	38%	6010	3020	0.0488	0.0488	1.047
UGC	34%	3246	2992	0.0799	0.0473	1.015
ESO	19%	2412	2187	0.109	0.0361	0.775
ESGC	9%	1351	1203	0.195	0.0570	1.223

TABLE 1

Numbers of galaxies, densities, and catalogue weights for the catalogues used in the ORS density field analysis. The *IRAS* values include only the portion of the survey outside the accepted ORS volumes; the *IRAS* sky coverage is 100% for $cz > 8000 \text{ km s}^{-1}$. The full-sky *IRAS* density for $cz < 8000 \text{ km s}^{-1}$ (optimal for minimum-variance estimates of the density) is $n_{IRAS} = 0.0466 \text{ h}^3 \text{ Mpc}^{-3}$.

for details). The maps below were constructed using the *IRAS* selection function, which, however, is not a very good approximation to the ORS selection functions for $cz > 8000 \text{ km s}^{-1}$. To gauge the importance of the differing catalogue selection functions in the rocket effect correction, we have compared the ORS peculiar flow field using both ϕ_{UGC} and ϕ_{IRAS} . (Differences among the three ORS selection functions are negligible in comparison to the difference between ORS and *IRAS*.) Although the rocket effect correction is substantial over the redshifts of interest, the ϕ_{UGC} and ϕ_{IRAS} flow fields are identical (to within $\sim 30 \text{ km s}^{-1}$, with negligible systematic differences over the sky) for $cz < 8000 \text{ km s}^{-1}$, where the selection functions behave similarly. At greater distances, however, the fields diverge dramatically, particularly in the dipole. Because we use only *IRAS* data for $cz > 8000 \text{ km s}^{-1}$, we are fortunately able to avoid this complication.

4. COMPARISON OF THE FIELDS

A detailed statistical comparison of the ORS and *IRAS* gravity fields is difficult due to the limited sky coverage of the ORS. Because we require an all-sky catalogue for the spherical harmonic analysis, we have filled in the Galactic plane with *IRAS* galaxies; the two fields are therefore not independent over the whole sky. In addition, the ORS shares some galaxies in common with the *IRAS* survey. Nevertheless, the qualitative comparison of the two fields can tell us whether or not improved redshift surveys might provide a better match to the Mark III data than DNW96 found for the *IRAS* survey. Detailed Wiener-filtered reconstructions of the *IRAS* density and gravity field in *real* space have been carried out (Webster, Lahav & Fisher 1997; see also Strauss & Willick 1995); our analysis, however, is done entirely in redshift space.

4.1. ORS and IRAS Density Fields

The density field contours on several radial shells are illustrated in Figure 1, where it is apparent that the ORS and *IRAS* fields are qualitatively very similar (compare with the similar figures in Santiago et al. 1995). The *IRAS* survey's under-counting of cluster centers is most evident on the near ($cz = 1000 \text{ km s}^{-1}$) radial slice, which contains Virgo ($\ell = 284^\circ$, $b = 75^\circ$), Ursa Major ($\ell = 145^\circ$, $b = 66^\circ$), and Fornax ($\ell = 237^\circ$, $b = -54^\circ$). With the Gaussian smoothing for this shell ($\sigma = 345 \text{ km s}^{-1}$), the ORS over-density for Virgo is $\delta^g \approx 10$, compared with

$\delta^g \approx 6.7$ in the *IRAS* field (recall that the smoothing increases with radius, so density contrasts appear smaller on more distant shells). Note that if the *IRAS* galaxies differed from the ORS galaxies only by an extra bias factor of $2/3$, which would match the peak Virgo over-densities for the two fields, then we would expect that a comparison of observed peculiar velocities with the ORS gravity field would yield a value of β lower than the corresponding number for the *IRAS* gravity field by the same factor.

On the next redshift slice ($cz = 3000 \text{ km s}^{-1}$), the Hydra-Centaurus complex is clearly visible around ($\ell = 300^\circ$, $b = 20^\circ$). The maximum over-densities are approximately 25% smaller for *IRAS* than for ORS. However, the smoothing on this shell is somewhat larger ($\sigma = 550 \text{ km s}^{-1}$), and the clusters are quite near the ORS $b = 20^\circ$ cutoff. The linear structure of the Supergalactic Plane is visible near $\ell = 135^\circ$, and there are pronounced voids ($\delta^g \approx -0.9$) towards $\ell = 265^\circ$, $b = -50^\circ$ and $\ell = 5^\circ$, $b = 10^\circ$.

At $cz = 5000 \text{ km s}^{-1}$, the Perseus-Pisces region around ($\ell = 140^\circ$, $b = -25^\circ$) is clearly much better sampled by the ORS survey than by the *IRAS* survey, but the qualitative features of the two fields are identical. The smoothing at this redshift is 815 km s^{-1} . The $b < -20^\circ$ parts of the Pavo-Indus-Telescopium region are also visible near $\ell = 330^\circ$. The density contrasts on more distant shells are much less pronounced, and beyond 8000 km s^{-1} the two fields are identical by construction.

4.2. Predicted Flow Fields

Figure 2 shows the *IRAS*- and ORS-predicted radial peculiar velocity fields (Local Group frame) on redshift shells for $\beta = 0.6$ (note these are not the same as the redshift shells in Fig. 1). Again, the overall agreement of the fields is quite good. The nearby shell ($cz = 500 \text{ km s}^{-1}$) is dominated by Virgo-centric infall, with galaxies towards Virgo and galaxies in the opposite direction of the sky flowing away from us. The ORS-predicted flow towards Virgo is approximately twice as large as the *IRAS*-predicted flow for the same value of β . There are also substantial ($v \gtrsim 300 \text{ km s}^{-1}$) predicted flows towards us from the Supergalactic poles, but the differences in these regions between the ORS and *IRAS* predictions are more modest than for the flow toward Virgo.

At $cz = 2000 \text{ km s}^{-1}$, the dipole component of the flow begins to dominate as a result of the motion of the Local Group, with infall on the back side of Virgo and outward

flow in the opposite direction. The flow of galaxies away from us as it falls into Hydra-Centaurus is modest but visible at this redshift. The dipole pattern grows with redshift, as evident in Figure 2c, and except for an overall scaling and slight change of orientation, the differences between the ORS and *IRAS* fields diminish.

The monopole, dipole, and quadrupole terms as a function of radius for the ORS- and *IRAS*-predicted flow fields are shown in Figures 3–5 for the same value $\beta = 0.6$, the high end of the “most likely” range of DNW96. The quantity plotted is c_{lm} , as defined in Appendix A. As emphasized by Davis (1998) and Nusser & Davis (1994), the monopole and dipole terms at a given redshift are sensitive only to the interior mass distribution, which should be well sampled. Tidal fields introduced by errors in the density field of the dilutely sampled exterior region will only affect the quadrupole and higher multipoles. Statistically significant disagreement between the measured and predicted velocity field for the dipole component is thus a sign that something is amiss, either a systematic error in one or both of the catalogues, incorrect treatment of an important component of non-linear flow, or non-uniform relative bias in the galaxy distribution. These figures compare the multipole moments of the *IRAS*- and ORS-predicted velocity fields, to see whether the DNW96 discrepancy continues to hold for the ORS data.

The ORS-predicted dipole terms (Fig. 4) are all significantly larger than the *IRAS*-predicted terms. The differences in the Galactic X ($m = 1$) and Y ($m = -1$) components arise primarily behind Perseus-Pisces, but the Z ($m = 0$) difference is mainly due to Virgo. The quadrupole terms agree quite well, except that the $m = -1$ magnitude is somewhat lower in *IRAS*, and the ORS data resolve the $m = 0$ peak around Perseus-Pisces a bit more sharply. We should point out that because each of the ORS subsamples are normalized to the *IRAS* density field (eq. [3]), the *IRAS* and ORS dipoles are not as statistically independent as we would otherwise like them to be.

Figures 3–5 also show the results when the ORS β value is lowered from 0.6 to 0.4. Note that equation 4 is only linear in β in the limit $\beta \rightarrow 0$. For β of order unity, redshift distortions lead to more complex behavior; thus the $\beta = 0.6$ and $\beta = 0.4$ ORS multipole terms are not simply proportional to each other. The overall amplitude of the ORS-predicted dipole for $\beta = 0.4$ agrees extremely well with the *IRAS*-predicted dipole for $\beta = 0.6$, but the increased weight of Virgo enhances the relative strength of the Z -component. Lowering the value of β has a fairly modest effect on the quadrupole terms, although the peak in the overall quadrupole amplitude at 2500 km s^{-1} is significantly reduced. The $m = -1$ component is brought into excellent agreement with the *IRAS* prediction, and the $m = \pm 2$ amplitudes are lowered somewhat below the *IRAS* prediction. In any case, the incorporation of the ORS data has worked in the wrong direction to correct the *IRAS*–Mark III dipole residual of DNW96, because the Y component of the Mark III field is much too small relative to the *IRAS* prediction, and the ORS data only drive these components further out of agreement.

The dipole of the *IRAS*-predicted velocity field does not seem to converge to the CMB dipole ($\ell = 268^\circ$, $b = 27^\circ$ in the LG frame) particularly well (Strauss et al. 1992c;

Webster et al. 1997); it consistently points about 30° away. With their larger Virgo-centric infall, the ORS data only exacerbate this situation. At $cz = 6000 \text{ km s}^{-1}$, the ORS dipole points to $\ell = 250^\circ$, $b = 55^\circ$, about 15° higher in latitude than the *IRAS* dipole. This is reflected in the larger magnitude of the $l = 1, m = 0$ multipole component of the field (Fig. 4), which points in the Galactic Z direction.

4.3. Predictions for Mark III Galaxies

The predicted peculiar velocities for the Mark III galaxies in three redshift slices are plotted in Figures 6–8. The *IRAS* plots differ from those in DNW96 only in the projection used and the orientation of the longitude coordinate. Note that the *IRAS* predictions use $\beta = 0.6$ while ORS uses $\beta = 0.4$, consistent with the apparent relative bias of the two fields of a factor of 1.5 (Strauss et al. 1992b; Hermit et al. 1996). In general, the difference between the ORS- and *IRAS*-predicted fields is quite small. In fact, the magnitude of these residuals is generally lower than the residuals seen by DNW96 in their tests on mock catalogues. The strong velocity shear seen in the Mark III sample across the Hydra-Centaurus complex is plainly absent from either of the redshift surveys; indeed, this region shows only very small differences between the fields. The largest systematic differences are seen for Perseus-Pisces; our peculiar motion away from this complex is smaller in the ORS-predicted field. The detailed statistical analysis of DNW96 shows discrepancies between *IRAS* and Mark III which would not be alleviated by our ORS gravity field.

4.4. Effects of Non-linear Bias

In general, the bias of the galaxy distribution is the function which relates fluctuations in the galaxy number density $\delta\rho^g$ to fluctuations in the overall matter distribution $\delta\rho$. The functional form depends on the details of galaxy formation, which are poorly understood. For simplicity, it is usually taken to be a linear function independent of scale, so that the bias parameter b has a single numerical value. Semi-analytic work (Kauffman, Nusser, & Steinmetz 1997; see also Weinberg 1995) suggests that most physical bias mechanisms lead to a nearly linear bias on large scales, but the value of the bias depends quite strongly on the power spectrum, galaxy type, and galaxy luminosity in a given sample. This is of course problematic for flux-limited surveys, in which the most distant galaxies are also the most luminous. The ORS data in fact show some evidence of a weakly scale-dependent bias (Hermit et al. 1996).

Provided that the bias is linear, our technique will recover the value of $\beta \approx \Omega^{0.6}/b$. Non-linear bias in the galaxy distribution will introduce systematic errors in the analysis. We investigate the impact of a non-linear bias by postulating a gridded mass density fluctuation field $\delta = [\mathcal{B}(\delta^g) - \bar{\mathcal{B}}]/b$, where \mathcal{B} is some non-linear function. The mean value $\bar{\mathcal{B}}$ over the set of grid points must be subtracted because the fluctuation field has zero mean by definition.

Most prescriptions for non-linear bias are functions of the local over-density δ . With the variable smoothing of our computed density field, however, it is difficult to implement such a non-linear bias in a spatially uniform fashion. But the mean value of the field is $\delta = 0$ independent of

smoothing, and it is therefore possible to construct a non-linear bias using $\delta = 0$ as a pivot. A simple non-linear form is the piecewise linear function

$$\mathcal{B}(\delta^g) = \begin{cases} \delta^g & \delta^g > 0 \\ (2/3)\delta^g & \delta^g \leq 0 \end{cases}, \quad (6)$$

as shown in Figure 9. This in effect makes galaxies more strongly clustered than dark matter in over-dense regions, and less strongly clustered in under-dense regions, relative to the case of linear bias. In other words, we are stealing dark matter from the clusters, filling the voids with more than would be expected on the basis of the galaxy distribution. The galaxy voids are thus substantially deeper than the matter voids for reasonable values of b (Cen & Ostriker 1992, 1993). This is plausible (though admittedly ad hoc) because galaxy formation is expected to be more efficient in dense regions, and it is consistent with the results of simulations (White et al. 1987; Dekel 1997; Lemson et al. 1998). We emphasize that our crude piecewise linear bias is only meant to be illustrative; a more complex algorithm could not readily be implemented because of the variable smoothing of our density field.

Even the fairly dramatic “knee” we have introduced in the bias at $\delta^g = 0$ has quite a modest effect on the predicted flow field. The overall amplitude of the flow is reduced, as expected because the dark matter distribution is now less clustered. However, the magnitude of this reduction is only $\sim 10\%$ (see Fig. 9), and the best-fit value of β would therefore only increase slightly. The direction of the dipole is altered by only $\sim 2^\circ$, and other qualitative features of the flow field are unchanged. It seems quite unlikely that even a rather extreme uniform bias prescription could plausibly eliminate the coherent residuals seen between Mark III and our predicted velocity fields.

5. CONCLUSIONS

The gravity field derived from the ORS is quite similar to the field derived from the *IRAS* survey, provided the value of β is multiplied by a factor of $\approx 2/3$, roughly consistent with the relative strength of clustering in the two surveys. Some differences from this simple scaling are observed; most significantly, the dipole of the ORS-predicted flow field is rotated towards Virgo and is further than the *IRAS* prediction from the CMB dipole. This non-scaling behavior arises because the ratio of ORS to *IRAS* density fluctuations is larger in the local Supercluster than in other regions.

DNW96 have found systematic discrepancies between the Mark III and *IRAS*-predicted flow fields, particularly a large coherent dipole residual, which cannot be physical because the dipole field depends only on the interior mass

distribution. Estimating the gravity field from the ORS survey has provided a check on the influence of the known shortcomings of the *IRAS* catalogue (namely, its sparse sampling and under-representation of cluster cores). Since the *IRAS* and ORS gravity fields are so similar, we conclude that the redshift-space catalogues are not themselves the source of the DNW96 discrepancies.

Compared to *IRAS*, the ORS gravity field will generally push us towards lower values of β in order to fit a given sample of peculiar velocity measurements. The result of DNW96 for the *IRAS*-Mark III comparison would then suggest $\beta \lesssim 0.45$, but this comparison with Mark III remains suspect due to the substantial quantitative discrepancies between the *IRAS* and Mark III fields. da Costa et al. (1998), on the other hand, showed that the SFI sample agrees quite well with the *IRAS* gravity field for $\beta = 0.6$; presumably this sample would also be consistent with the ORS field for $\beta \approx 0.4$. Another serious concern for the Mark III comparison is the fact that complementary methods for attacking the velocity field problem have not converged to a consistent, unambiguous result. The POTENT analysis of Sigad et al. (1998) and Dekel et al. (1993) favors larger values ($\beta \sim 1$) than the ITF and VELMOD analyses. These methods weight the data in very different ways, and given that the fields show some level of inconsistency, it is not surprising that different analyses of the same data yield different answers.

The sources of the DNW96 discrepancies between the *IRAS* gravity field and the Mark III peculiar velocity measurements remain uncertain. These discrepancies might be telling us that galaxies cluster in a way which is not closely related to the clustering of the mass, or that the linear gravitational instability model provides an inadequate description of flows on the scales of interest. Alternatively, there may be unknown systematic biases in the Mark III data; see also the discussion in Willick & Strauss (1998). We have investigated a simple but plausible generalization of the usual linear bias model for galaxy clustering, but this does not significantly affect features in the predicted velocity field; even a rather sizeable change in the slope of the bias relation at $\delta^g = 0$ causes only a modest reduction in the amplitude of the field. Improved full-sky peculiar velocity surveys (e.g., Strauss 1997) of larger galaxy samples are eagerly awaited. Such surveys are quite a difficult undertaking, but they may go some way towards clarifying our understanding of large-scale flows in the universe.

J. E. B. acknowledges support from an NSF graduate fellowship. This work was supported in part by NSF grant AST95-28340. M. A. S. acknowledges the support of the Alfred P. Sloan Foundation, Research Corporation, and NSF grant AST96-16901.

APPENDIX

SPHERICAL HARMONIC FORMALISM

We solve for the linear peculiar velocity field from the density field expanded in spherical harmonics on radial (redshift) shells. The conventional spherical harmonics are defined to be

$$Y_{lm}(\theta, \varphi) \equiv K_{lm} P_{lm}(\cos \theta) e^{im\varphi}, \quad (A1)$$

where

$$K_{lm} \equiv \left[\frac{2l+1}{4\pi} \frac{(l-m)!}{(l+m)!} \right]^{1/2} \quad (\text{A2})$$

and the P_{lm} 's are the associated Legendre polynomials. Since the density and velocity fields are real, it is convenient to work with the real-valued spherical harmonic functions, which differ slightly from their complex cousins. Following Bunn (1996), we define them as

$$\mathcal{Y}_{lm} \equiv (-)^m K_{lm} P_{lm}(\cos \theta) \times \begin{cases} 1 & m = 0 \\ \sqrt{2} \cos m\varphi & m > 0 \\ \sqrt{2} \sin |m|\varphi & m < 0. \end{cases} \quad (\text{A3})$$

The coefficients a_{lm} of an arbitrary real field $A(\mathbf{s})$ are related to the field by

$$a_{lm}(s) = \int d\Omega \mathcal{Y}_{lm} A(\mathbf{s}) \quad (\text{A4})$$

$$A(\mathbf{s}) = \sum_{l=0}^{\infty} \sum_{m=-l}^l a_{lm}(s) \mathcal{Y}_{lm}. \quad (\text{A5})$$

It is convenient to normalize the coefficients of multipole order l by the value of \mathcal{Y}_{l0} at the North Galactic Pole; we therefore define

$$c_{lm} \equiv \left(\frac{2l+1}{4\pi} \right)^{1/2} a_{lm}. \quad (\text{A6})$$

With this normalization, c_{11} is the amplitude of the dipole vector projected along the Galactic X axis ($\ell = b = 0^\circ$), $c_{1,-1}$ is the amplitude along the Y axis ($\ell = 90^\circ$, $b = 0^\circ$), and c_{10} is the amplitude along the Z axis ($b = 90^\circ$). The amplitude of the dipole is the quadrature sum of the three coefficients. The quadrupole terms of the real-valued spherical harmonics are

$$\mathcal{Y}_{20} = \frac{1}{4} \sqrt{\frac{5}{\pi}} (3 \cos^2 \theta - 1) \quad (\text{A7})$$

$$\mathcal{Y}_{21} = \frac{1}{4} \sqrt{\frac{15}{\pi}} \sin 2\theta \cos \varphi \quad (\text{A8})$$

$$\mathcal{Y}_{2,-1} = \frac{1}{4} \sqrt{\frac{15}{\pi}} \sin 2\theta \sin \varphi \quad (\text{A9})$$

$$\mathcal{Y}_{22} = \frac{1}{4} \sqrt{\frac{15}{\pi}} \sin^2 \theta \cos 2\varphi \quad (\text{A10})$$

$$\mathcal{Y}_{2,-2} = \frac{1}{4} \sqrt{\frac{15}{\pi}} \sin^2 \theta \sin 2\varphi, \quad (\text{A11})$$

where Galactic longitude is $\ell = \varphi$ and latitude is $b = 90^\circ - \theta$.

ROCKET EFFECT CORRECTIONS

A limitation of constructing a merged density field out of different catalogues and then solving for the velocity field is that equation (4) only allows for a single radial selection function in the rocket effect term (Kaiser 1987). This term corrects for the fact that, when constructing the density field, we have evaluated the selection function ϕ at each galaxy's redshift rather than its (unknown) distance. This can be a substantial correction to the redshift-space density field (Fisher et al. 1995b).

For the ORS survey, unfortunately, the selection function $\phi(\mathbf{s})$ is not independent of angle on the sky, but depends on the catalogue and the extinction along the line of sight. The linear equation for the velocity potential Φ of Nusser & Davis (1994) is

$$\frac{1}{f} \nabla^2 \Phi + \frac{1}{s^2} \frac{\partial}{\partial s} \left(s^2 \frac{\partial \Phi}{\partial s} \right) = \frac{1}{b} \left(\delta^g - \frac{1}{s} \frac{\partial \ln \phi}{\partial \ln s} \frac{\partial \Phi}{\partial s} \right), \quad (\text{B1})$$

where $f \approx \Omega^{0.6}$, b is the bias, and δ^g is the galaxy over-density in redshift space. A general selection function which is a function of position on the sky (θ, φ) will introduce couplings between different modes of the spherical harmonic expansion. Expanding Φ on each redshift shell as

$$\Phi(\mathbf{s}) = \sum_{l=0}^{\infty} \sum_{m=-l}^l \Phi_{lm}(s) Y_{lm}(\theta, \varphi) \quad (\text{B2})$$

and similarly for δ^g , multiplying through by Y_{lm}^* and integrating over solid angle, we find that the term subtracted from δ^g in equation (4) becomes

$$-\frac{1}{s} \sum_{l'=0}^{\infty} \sum_{m'=-l'}^{l'} u_{l'm'} \int_{(4\pi)} d(\cos \theta) d\varphi Y_{lm}^* Y_{l'm'} \frac{\partial \ln \phi}{\partial \ln s}, \quad (\text{B3})$$

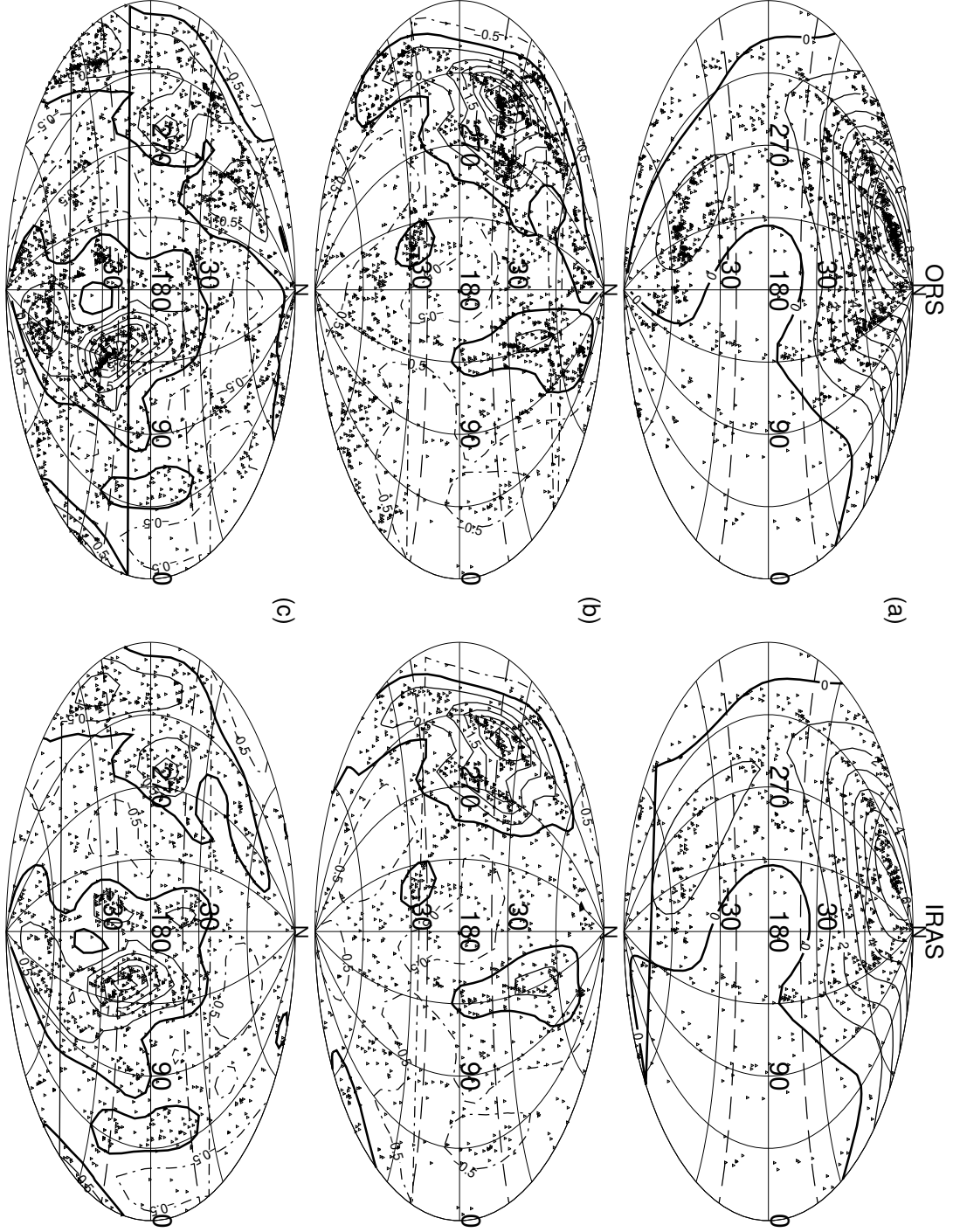
where $u \equiv -\partial\Phi/\partial s$ is the radial peculiar velocity. For a selection function independent of azimuthal angle φ , this expression reduces to

$$-\frac{2\pi}{s} \sum_{l' \geq m} u_{l'm} K_{lm} K_{l'm} \int_{-1}^1 d(\cos \theta) P_{lm} P_{l'm} \frac{\partial \ln \phi}{\partial \ln s}. \quad (\text{B4})$$

This expression replaces the $-(u_{lm}/s)(d \ln \phi / d \ln s)$ term in equation (4). For our catalogues, the angular dependence of the selection function is approximately just a step discontinuity at $|b| = 20^\circ$, so by symmetry, even (odd) values of l' make no contribution to odd (even) values of l . The utility of the spherical harmonic expansion breaks down unless the $l' = l$ term is dominant. For the analysis at $cz < 8000 \text{ km s}^{-1}$, the corrections are negligible because the ORS and IRAS selection functions track each other quite well. A deeper analysis, or one in which the selection functions of the merged catalogues are not so similar, may need to take account of these corrections.

REFERENCES

- Bunn, E. T. 1996, PhD Thesis, University of California, Berkeley
 Burstein, D. & Heiles, C. 1984, ApJS, 54, 33
 Canavezes, A. et al. 1998, MNRAS, in press (astro-ph/9712228)
 Cen, R. & Ostriker, J. P. 1992, ApJ, 399, L113
 Cen, R. & Ostriker, J. P. 1993, ApJ, 417, 415
 da Costa, L. N., Nusser, A., Freudling, W., Giovanelli, R., Haynes, M. P., Salzer, J. J., & Wegner, G. 1998, MNRAS, in press (astro-ph/9707299)
 Davis, M. 1998, Proc. Natl. Acad. Sci., United States, 95, 78
 Davis, M., Nusser, A., & Willick, J. A. 1996, ApJ, 473, 22 (DNW96)
 Dekel, A. 1994, ARA&A, 32, 371
 Dekel, A. 1997, private communication
 Dekel, A., Bertschinger, E., Yahil, A., Strauss, M. A., Davis, M., & Huchra, J. 1993, ApJ, 412, 1
 Fisher, K. B., Davis, M., Strauss, M. A., Yahil, A., & Huchra, J. P. 1995a, ApJS, 100, 69
 Fisher, K. B., Lahav, O., Hoffman, Y., Lynden-Bell, D., & Zaroubi, S. 1995b, MNRAS, 272, 885
 Freudling, W., da Costa, L. N., & Pellegrini, P. S. 1994, MNRAS, 268, 943
 Giovanelli, R., Haynes, M. P., Herter, T., Vogt, N. P., da Costa, L. N., Freudling, W., Salzer, J. J., & Wegner, G. 1997, AJ, 113, 53
 Hermit, S., Santiago, B. X., Lahav, O., Strauss, M. A., Davis, M., Dressler, A., Huchra, J. P. 1996, MNRAS, 283, 709
 Hudson, M. J. 1993a, MNRAS, 265, 43
 Hudson, M. J. 1993b, MNRAS, 265, 72
 Kaiser, N. 1987, MNRAS, 227, 1
 Kauffman, G., Nusser, A., & Steinmetz, M. 1997, MNRAS, 286, 795
 Lahav, O., Fisher, K. B., Hoffman, Y., Scharf, C. A., Zaroubi, S. 1994, ApJ, 423, 93
 Lemson, G., Colberg, J. M., Kauffman, G., White, S. D. M., & Dekel, A. 1998, in preparation
 Mathewson, D. S., Ford, V. L., & Buchhorn, M. 1992, ApJS, 81, 413
 Nusser, A. & Davis, M. 1994, ApJ, 421, 1
 Peebles, P. J. E. 1980, The Large Scale Structure of the Universe (Princeton University Press, Princeton)
 Riess, A. G., Davis, M., Baker, J. E., & Kirshner, R. P. 1997, ApJ, 488, 1
 Santiago, B. X. & Strauss, M. A. 1992, ApJ, 387, 9
 Santiago, B. X., Strauss, M. A., Lahav, O., Davis, M., Dressler, A., & Huchra, J. P. 1995, ApJ, 446, 457
 Santiago, B. X., Strauss, M. A., Lahav, O., Davis, M., Dressler, A., & Huchra, J. P. 1996, ApJ, 461, 38
 Sigad, Y., Eldar, A., Dekel, A., Strauss, M. A., & Yahil, A. 1998, ApJ, 495, 516 (astro-ph/9708141)
 Stiening, R., Skrutski, M. F., & Capps, R. 1995, BAAS, 187.7508S
 Strauss, M. A. 1997, in Critical Dialogues in Cosmology, ed. N. Turok (Singapore: World Scientific), 423
 Strauss, M. A., Davis, M., Yahil, A., & Huchra, J. P. 1992b, ApJ, 385, 421
 Strauss, M. A., Huchra, J. P., Davis, M., Yahil, A., Fisher, K. B. & Tonry, J. 1992a, ApJS, 83, 29
 Strauss, M. A. & Willick, J. A. 1995, Phys Rep, 261, 271
 Strauss, M. A., Yahil, A., Davis, M., Huchra, J. P., & Fisher, K. 1992c, ApJ, 397, 395
 Strauss, M. A., et al. 1998, in preparation
 Webster, M., Lahav, O., & Fisher, K. B. 1997, MNRAS, 287, 425
 Weinberg, D. H. 1995, in Wide-Field Spectroscopy and the Distant Universe, ed. S. J. Maddox & A. Aragon-Salamanca (Singapore: World Scientific), 129
 White, S. D. M., Davis, M., Efstathiou, G., & Frenk, C. S. 1987, Nature, 330, 451
 Willick, J. A., Courteau, S., Faber, S. M., Burstein, D., Dekel, A., & Strauss, M. A. 1997a, ApJS, 109, 333
 Willick, J. A. & Strauss, M. A. 1998, ApJ, in press (astro-ph/9801307)
 Willick, J. A., Strauss, M. A., Dekel, A., & Kolatt, T. 1997b, ApJ, 486, 629
 Yahil, A., Strauss, M. A., Davis, M., & Huchra, J. P. 1991, ApJ, 372, 380
 Yahil, A., Tammann, G. A., & Sandage, A. 1977, ApJ, 217, 903



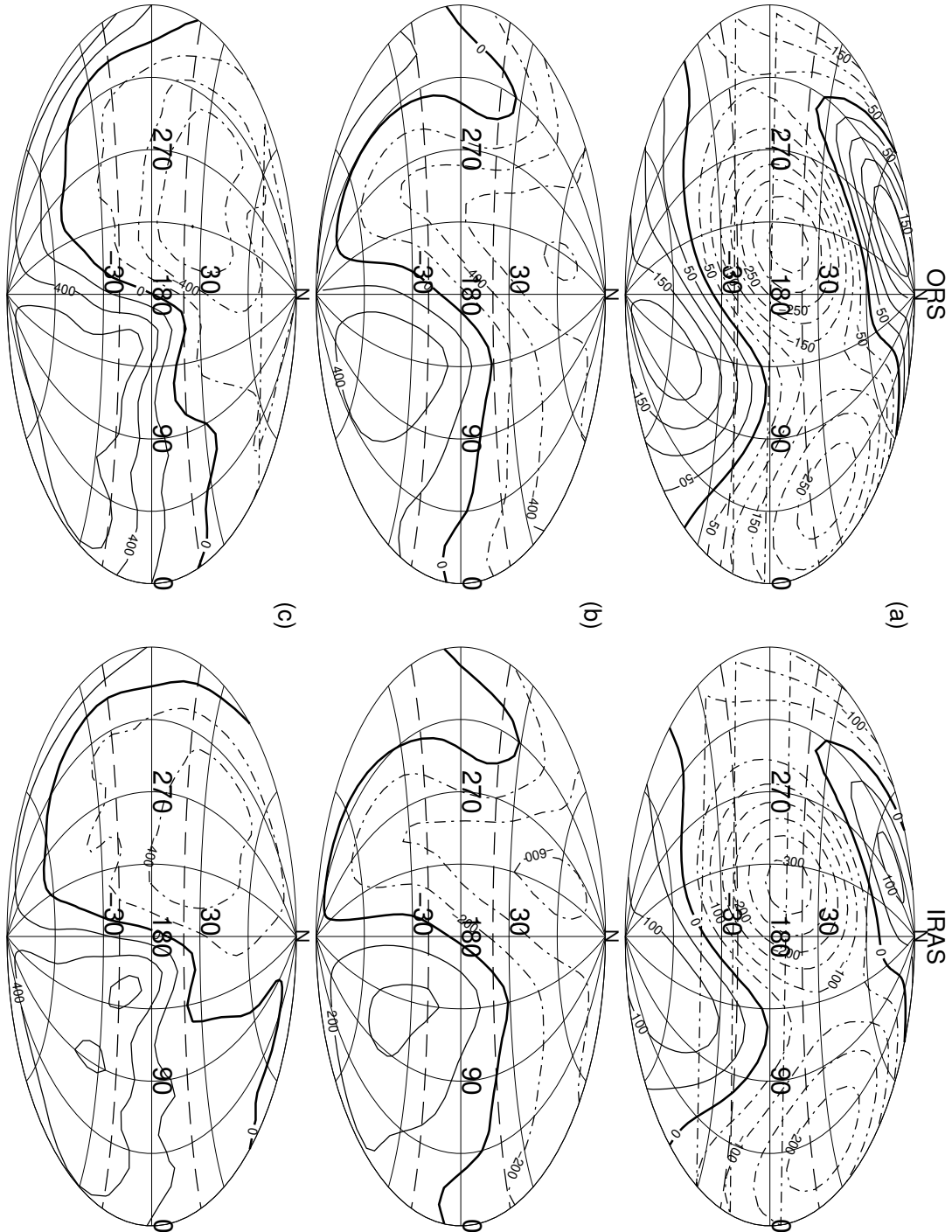


FIG. 2.— Radial slices of the ORS- and *IRAS*-predicted peculiar velocity fields in the Local Group frame for $\beta = 0.6$. Dot-dashed contours show negative (approaching the Local Group) velocities. (a) $cz = 500 \text{ km s}^{-1}$, contour spacing 50 km s^{-1} . (b) $cz = 2000 \text{ km s}^{-1}$, contour spacing 200 km s^{-1} . (c) $cz = 5000 \text{ km s}^{-1}$, contour spacing 200 km s^{-1} .

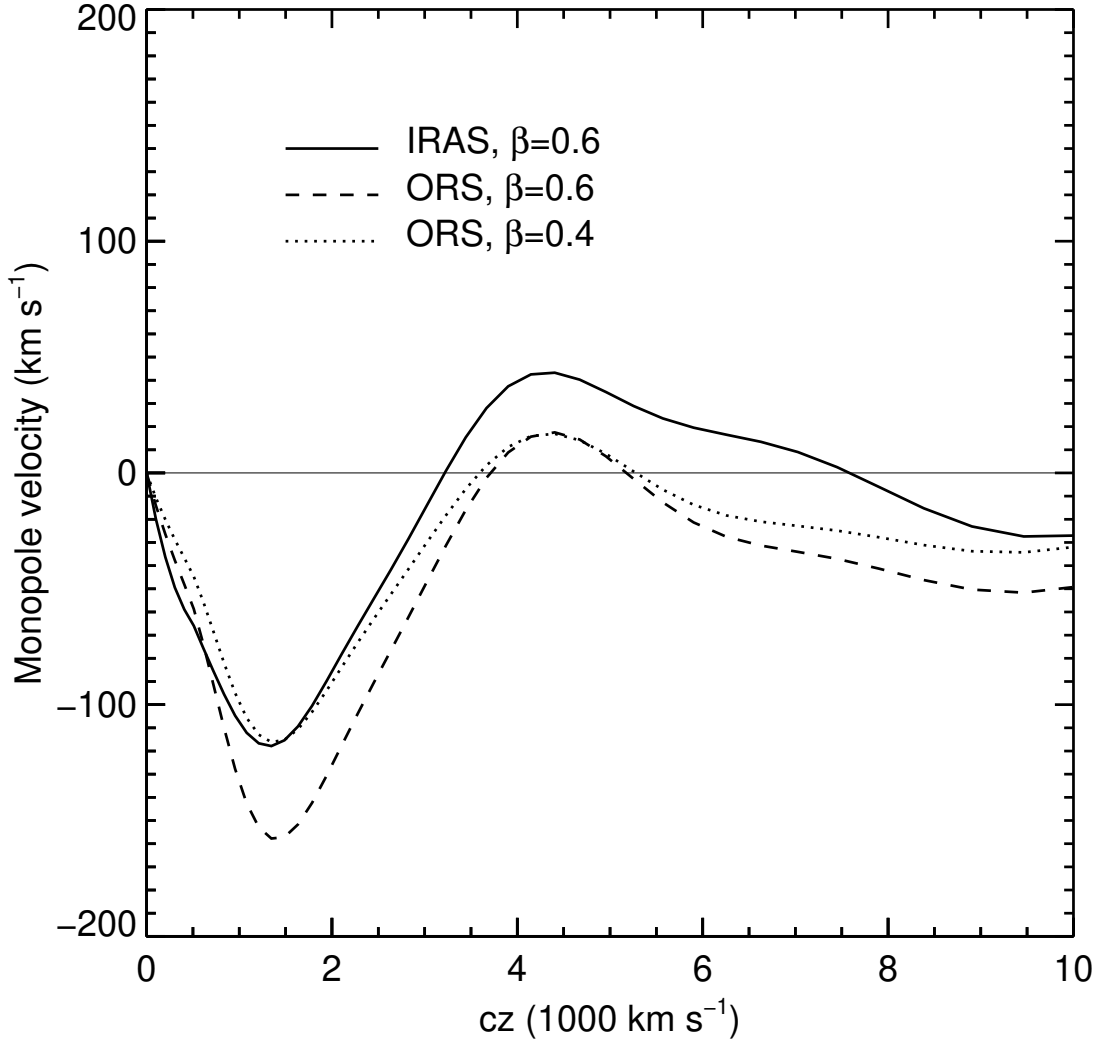


FIG. 3.— Monopole coefficient c_{00} of the real-valued spherical harmonic expansion of the ORS- and *IRAS*-predicted peculiar velocity fields. The solid line is the *IRAS*-predicted field for $\beta = 0.6$, the dashed line is the ORS-predicted field for the same β , and the dotted line is the ORS-predicted field when β is reduced to 0.4.

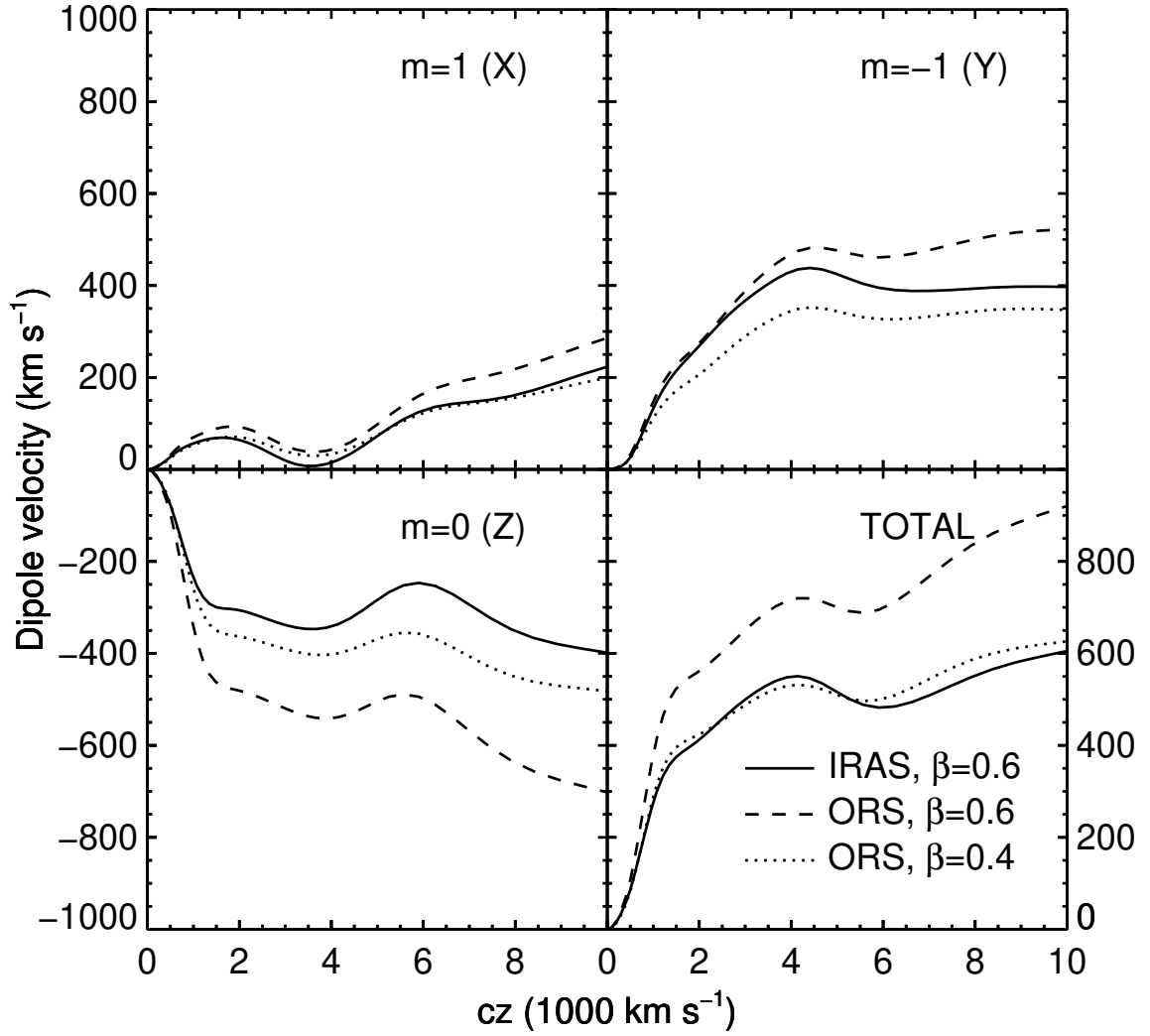


FIG. 4.— As in Figure 3, but for the dipole coefficients c_{1m} . The quadrature sum is shown in the lower right panel.

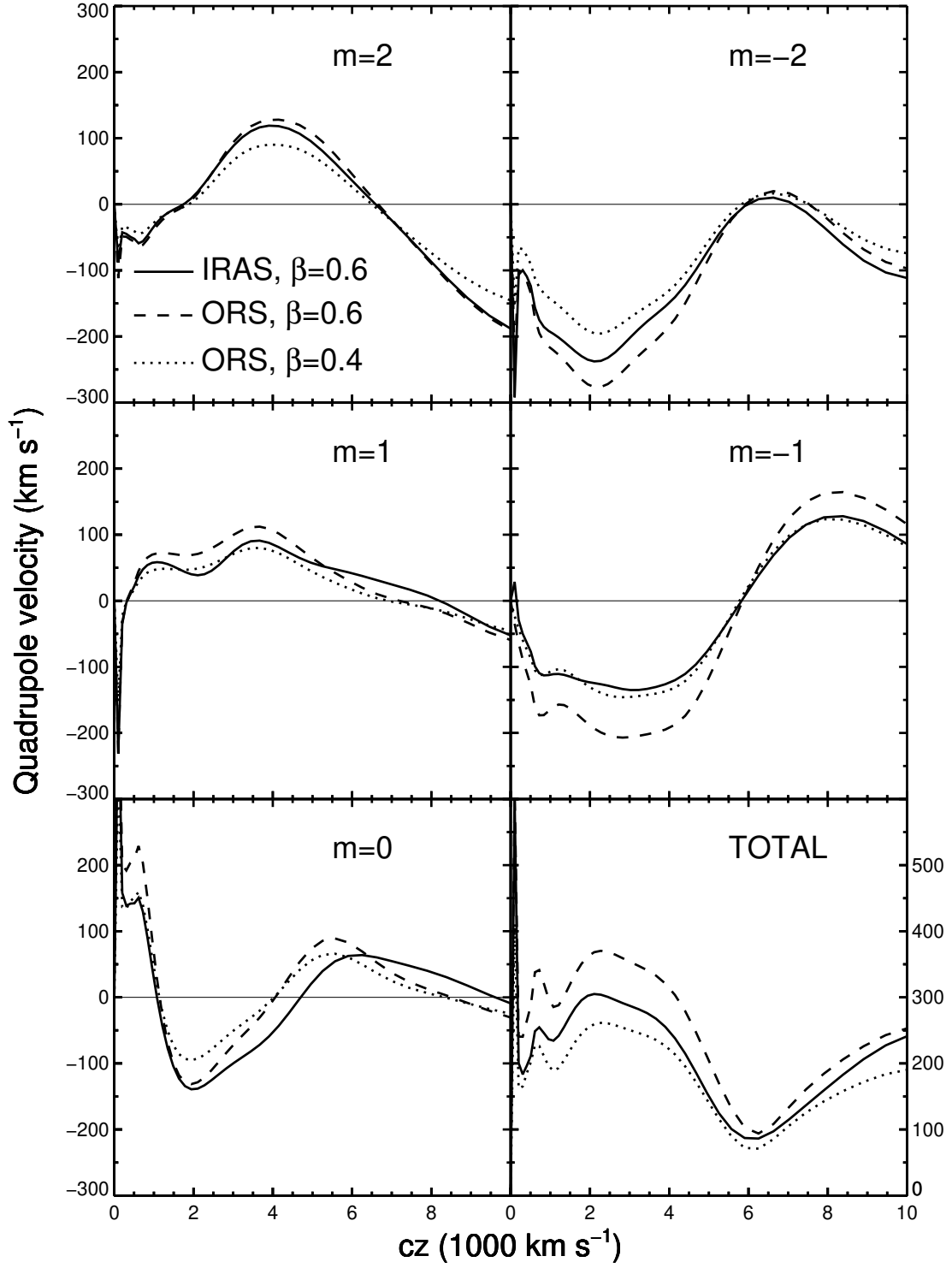


FIG. 5.— As in Figure 3, but for the quadrupole coefficients c_{2m} . The quadrature sum is shown in the lower right panel.

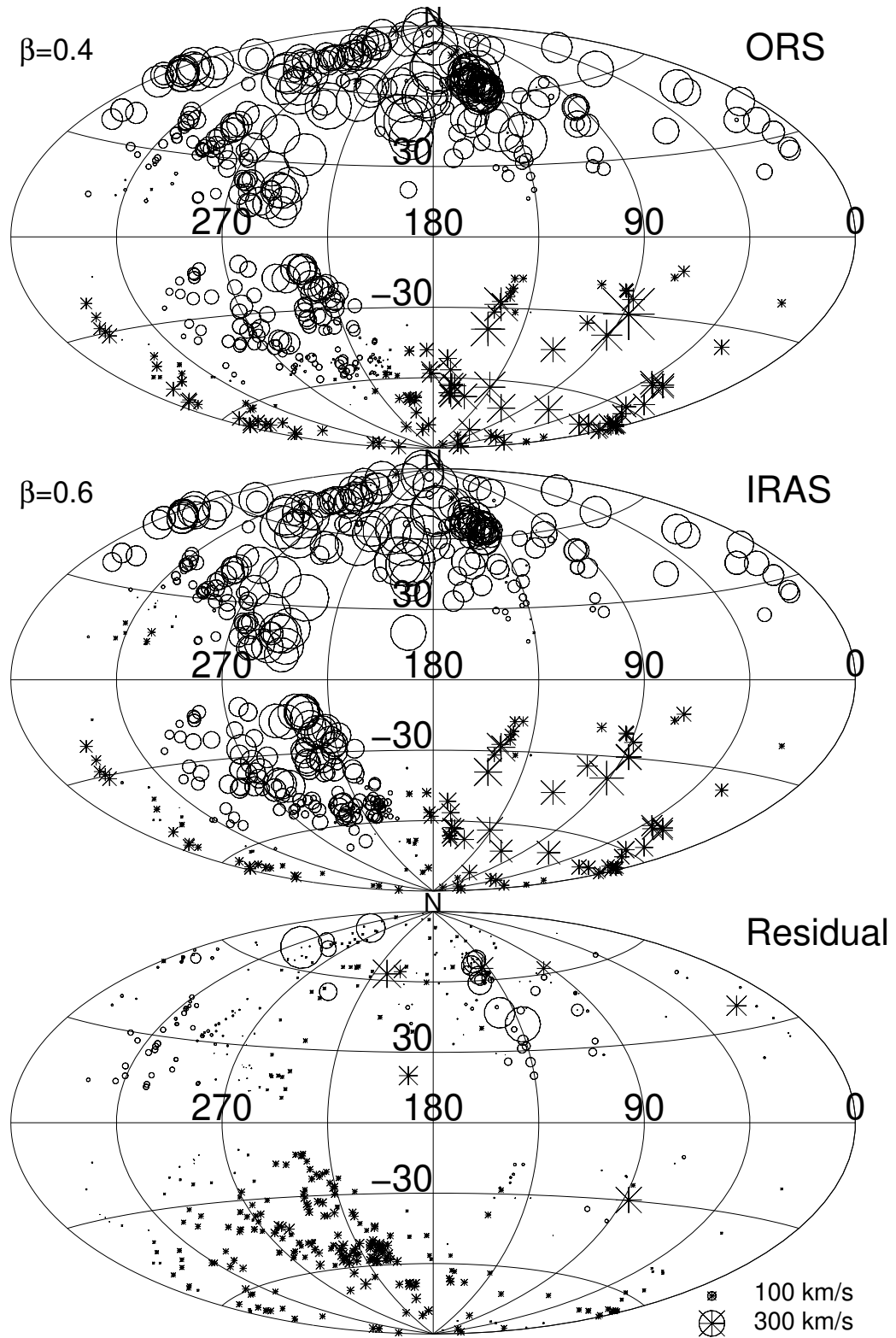


FIG. 6.— Predicted peculiar velocities for the Mark III galaxies based on ORS ($\beta = 0.4$, top) and IRAS ($\beta = 0.6$, middle) for the near redshift slice ($cz < 2000 \text{ km s}^{-1}$). Circles indicate positive peculiar velocities (directed away from the LG), and crosses indicate negative velocities. The bottom plot shows the difference between the ORS and IRAS predictions.

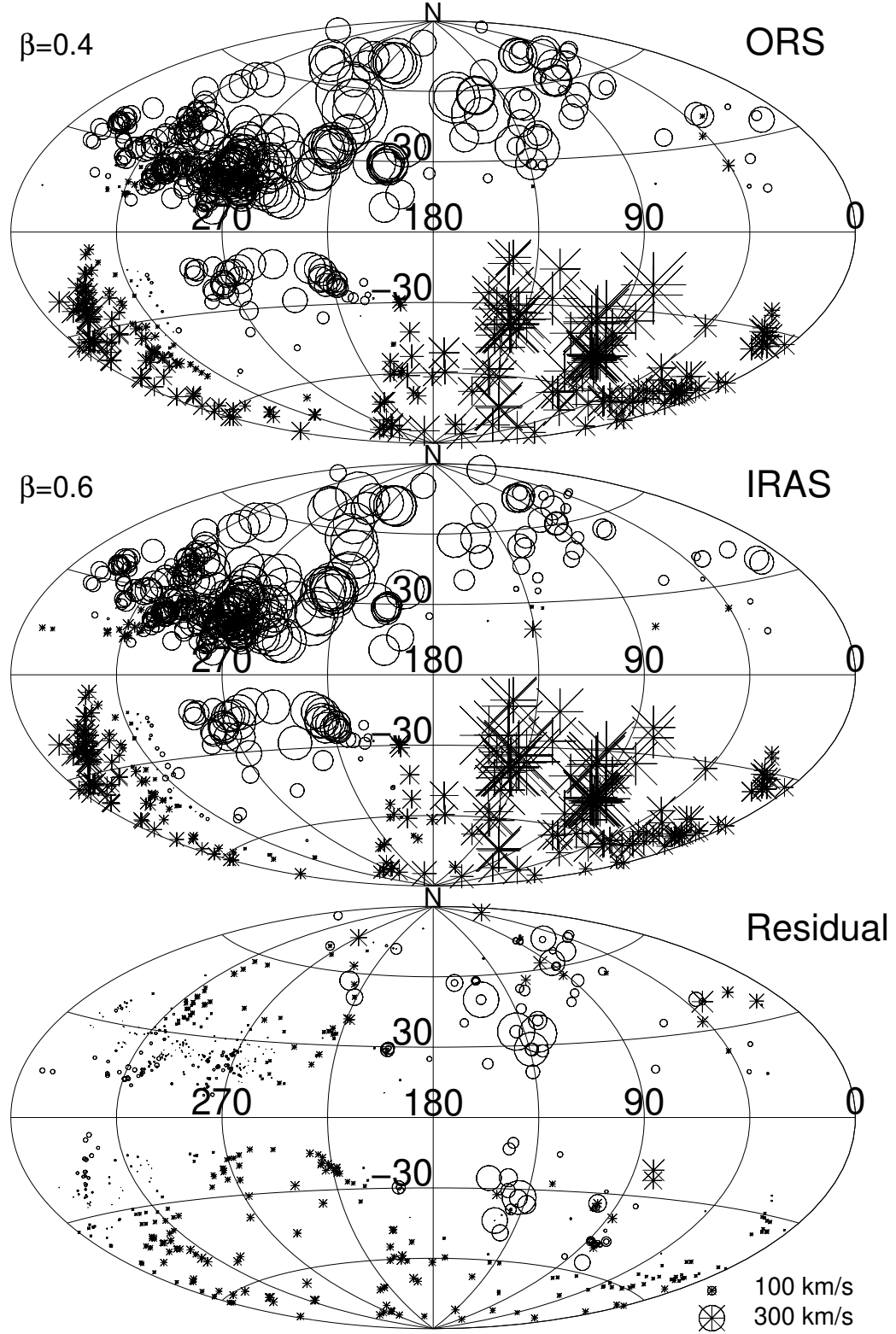


FIG. 7.— As in Figure 6, for the middle redshift slice ($2000 < cz < 4000 \text{ km s}^{-1}$).

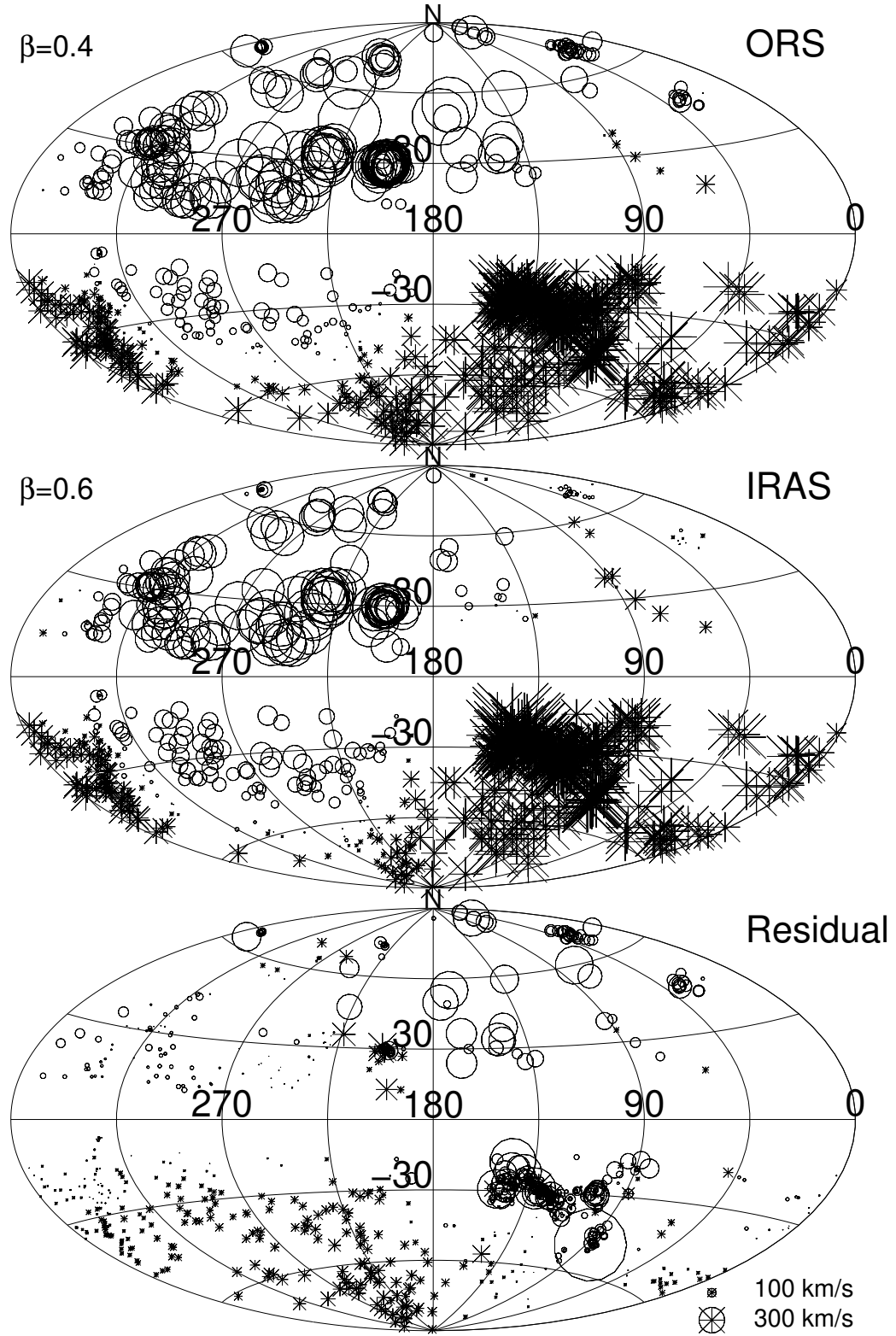


FIG. 8.— As in Figure 6, for the distant redshift slice ($4000 < cz < 6000 \text{ km s}^{-1}$).

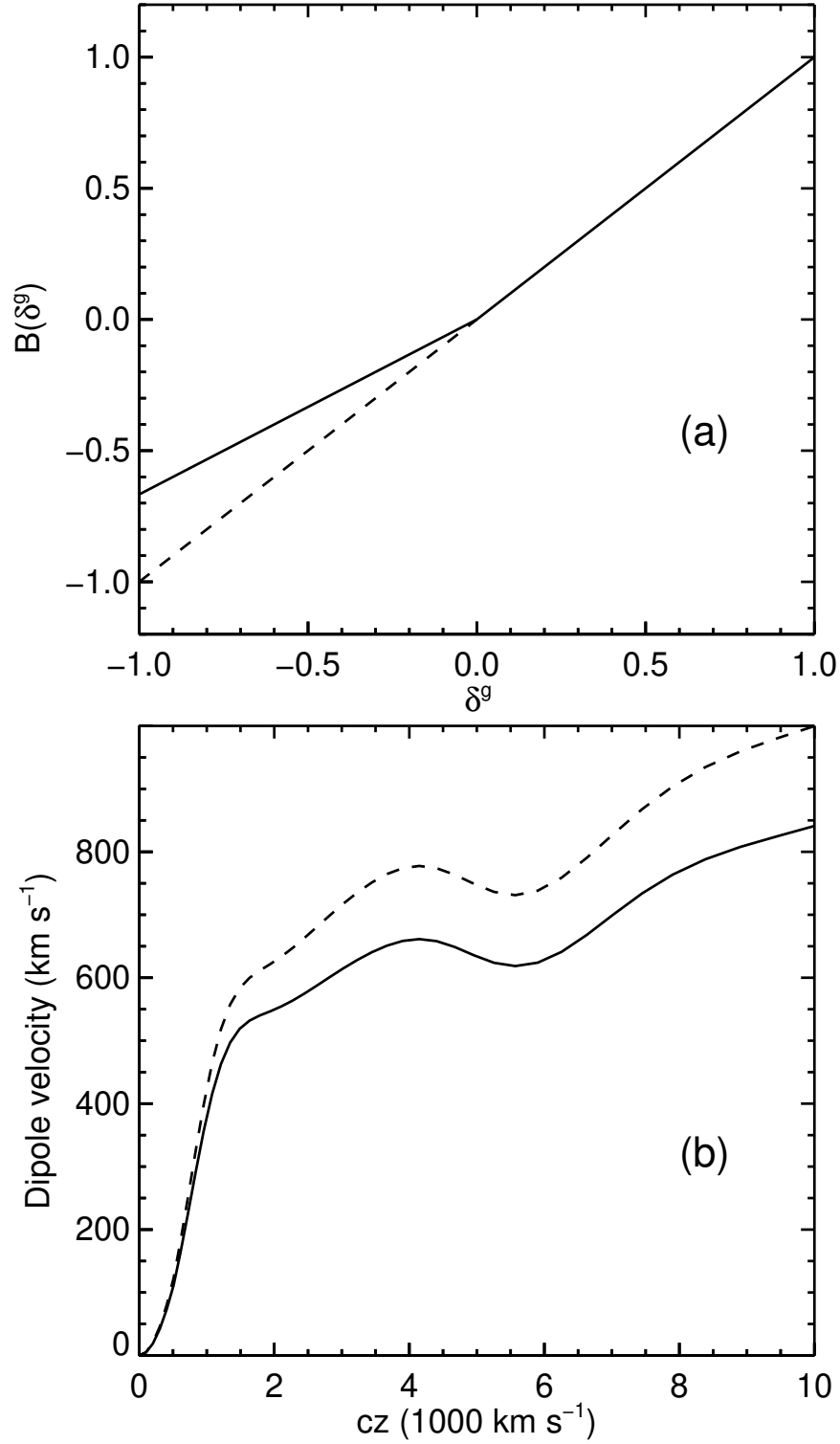


FIG. 9.— (a) A simple non-linear form for the bias function \mathcal{B} (solid line), consistent with our variable smoothing procedure. The fractional fluctuation in the galaxy density is δ^g . (b) Effect of the non-linear bias above on the dipole amplitude of the ORS peculiar flow field with $\beta = 0.6$. The dashed line is for linear bias.